JETIR.ORG ISSN: 2349-5162 | ESTD Year : 2014 | Monthly Issue
JOURNAL OF EMERGING TECHNOLOGIES AND INNOVATIVE RESEARCH (JETIR)
An International Scholarly Open Access, Peer-reviewed, Refereed Journal

Comparative study of turbulent nature of solar plasma during the solar cycle 23 and 24

[1]Anoop parsai

[1]Barkatullah University Bhopal

[2]Dr Harsha Jalori

[2]Shyama Prasad Mukharji Govt Benazeer College Bhopal

Abstract

Solar wind variability spans a wide range of amplitudes and timescales, from turbulent fluctuations to the 11 year solar cycle. We apply the data quantile-quantile (DQQ) method to NASA/Wind observations spanning solar cycles 23 and 24, to study how the uniqueness of each cycle maximum and minimum manifests in the changing statistical distribution of plasma parameters in fast and slow solar wind. The DQQ method allows us to discriminate between two distinct components of the distribution: the core region simply tracks the solar cycle in its moments but shows little sensitivity to solar wind state or the specific activity of each cycle. This would be consistent with an underlying in situ process such as turbulence driving the evolution of fluctuations up to an outer scale. In contrast, the tail component of the distribution is sensitive both to the differences between the maxima and minima of cycles 23 and 24, and the fast or slow state of the solar wind.

1. INTRODUCTION

In plasma physics terms, it is the cavity formed by the Sun in the surrounding interstellar medium. The "bubble" of the heliosphere is continuously "inflated" by plasma originating from the Sun, known as the solar wind. Outside the heliosphere, this solar plasma gives way to the interstellar plasma permeating the Milky Way galaxy.

Plasmas are found throughout the Solar System and beyond: in the solar corona and solar wind, in the magnetospheres of the Earth and other planets, in tails of comets, in the inter-stellar and inter-galactic media and in the accretion disks around black holes.

In recent years talks about the space weather (Singh et al. 2010) and solar activity (Loehle and Singer 2010; Siingh et al. 2011) have got increased impetus because of their decisive impact on terrestrial environment and climate change. Sunspots, regions of most intense magnetic fields on the surface of the Sun still have their relevance in solar and geomagnetic studies. Number of sunspots can increase or decrease over regular time scale of 11 year called solar or sunspot cycle. More sunspots mean increased solar activity. The highest number of sunspots in any given cycle is designated as solar maximum while the lowest number is designated as solar minimum. The last completed solar cycle 23 that ended in the year 2008 has been the subject of numerous studies, which have emphasized its unusual properties (de Jager and Duhau 2009; Agee et al. 2010; Russell et al. 2010; Singh et al. 2014). Whereas year 2008 and 2009 have shown solar minimum conditions while year 2011, 2012 and 2013 have been the year of solar maximum during half period of solar cycle 24. The solar radio flux at 10.7 cm (2800 MHz) has been an excellent indicator of solar activity. Usually called as the F10.7 cm index, it is one of the longest running records of solar activity (Kenneth 1990). The F10.7 radio emissions originates high in the chromosphere and low in the corona of the solar atmosphere. The F10.7 correlates well with the sunspot number as well as a number of ultra violet (UV) and visible solar irradiance records.

Turbulence

Turbulent fluids are characterized by rapidly fluctuating fluid parameters, such as pressure, flow speed and density. Two examples of turbulence in fluids are: atmospheric turbulence, which may cause bumpy airplane rides and the water behind the stern of a moving boat.

Turbulence in Plasma

Plasma is a state of matter where ions and electrons have not formed atoms, but exist side-by-side in an ionized gas. Plasma is the most abundant state of ordinary matter in the universe and it is often turbulent. Examples of turbulent astrophysical plasmas are the interstellar medium and the atmosphere of stars. More locally, turbulence is prevalent in several regions in our geospace, such as: the solar wind and ion foreshock region, the magnetosheath, the cusps, the magnetotail, and the ionosphere. Turbulence acts to transfer energy from large-scale motion into small scale motion and heat. In ordinary fluids, this energy dissipation is caused by viscosity in the fluid. In collisionless plasmas, however, energy is dissipated by particles interacting with waves in the plasma. Understanding turbulence is important because it influences particle heating and acceleration, such as solar energetic particles and cosmic rays. It is also important because it heavily influences the structure and dynamics of the Earth's magnetosphere as well as energy and mass inflow to the magnetosphere.

2. LITERATURE REVIEW

Dibyendu Nandy et. al. (2021) Predicting the properties of an upcoming solar cycle by using old cycle data has been attempted by various methods (see a detailed review by *Hathaway et al.* [1999, and references therein], A particularly popular current method [*Svalgaard et al.*, 2005; *Schatten*, 2005] involves the use of polar fields from previous cycles as "precursors", of the next cycle. Here we propose and test a new method, based on a flux transport dynamo model that has already been demonstrated to reproduce many solar cycle features [*Dikpati et al.*, 2004]. The dynamo-based scheme of *Schatten et al.* [1978] first attempted to make a physical connection between the strength of an upcoming sunspot cycle and the previous cycle's polar fields, assuming that there is a "magnetic persistence" between these two. Schatten et al.'s "magnetic persistence" was based upon a relation between the surface polar fields and the spot-producing toroidal fields, generated by differential rotation shearing (the Ω-effect). Implicit in this "dynamo based" approach is that the polar fields of the previous cycle can be sheared by the solar differential rotation in time to produce toroidal fields of the new cycle. [1]

S.T. Lepri et. al. (2013) Solar wind plasma and compositional properties reflect the physical properties of the corona and its evolution over time. Studies comparing the previous solar minimum with the most recent, unusual solar minimum indicate that significant environmental changes are occurring globally on the Sun. For example, the magnetic field decreased 30% between the last two solar minima, and the ionic charge states of O have been reported to change toward lower values in the fast wind. In this work, we systematically and comprehensively analyze the compositional changes of the solar wind during cycle 23 from 2000 to 2010 while the Sun moved from solar maximum to solar minimum. We find a systematic change of C, O, Si, and Fe ionic charge states toward lower ionization distributions. We also discuss long-term changes in elemental abundances and show that there is a ~50% decrease of heavy ion abundances (He, C, O, Si, and Fe) relative to H as the Sun went from solar maximum to solar minimum. During this time, the relative abundances in the slow wind remain organized by their first ionization potential. We discuss these results and their implications for models of the evolution of the solar atmosphere, and for the identification of the fast and slow wind themselves. [2]

E. Robbrecht *et al* (2009) In this paper, we present the first automatically constructed LASCO coronal mass ejection (CME) catalog, a result of the application of the Computer Aided CME Tracking software (CACTus) on the LASCO archive during the interval 1997 September–2007 January. We have studied the CME characteristics and have compared them with similar results obtained by manual detection (CDAW CME catalog). On average, CACTus detects less than two events per day during solar minimum, up to eight events during maximum, nearly half of them being narrow (<20°). Assuming a correction factor, we find that the CACTus CME rate is surprisingly consistent with CME rates found during the past 30 years. The CACTus

statistics show that small-scale outflow is ubiquitously observed in the outer corona. The majority of CACTus-*only* events are narrow transients related to previous CME activity or to intensity variations in the slow solar wind, reflecting its turbulent nature. A significant fraction (about 15%) of CACTus-*only* events were identified as independent events, thus not related to other CME activity. The CACTus CME width distribution is essentially scale invariant in angular span over a range of scales from 20° to 120° while previous catalogs present a broad maximum around 30°. The possibility that the size of coronal mass outflows follow a power-law distribution could indicate that no typical CME size exists, i.e., that the narrow transients are not different from the larger well defined CMEs. [3]

L.-L. Zhao et. al. (2016) Forbush decrease (FD) events are of great interest for transient galactic cosmic-ray (GCR) modulation study. In this study, we perform comparative analysis of two prominent Forbush events during cycle 24, occurring on 2012 March 8 (Event 1) and 2015 June 22 (Event 2), utilizing the measurements from the worldwide neutron monitor (NM) network. Despite their comparable magnitudes, the two Forbush events are distinctly different in terms of evolving GCR energy spectrum and energy dependence of the recovery time. The recovery time of Event 1 is strongly dependent on the median energy, compared to the nearly constant recovery time of Event 2 over the studied energy range. Additionally, while the evolutions of the energy spectra during the two FD events exhibit similar variation patterns, the spectrum of Event 2 is significantly harder, especially at the time of deepest depression. These difference are essentially related to their associated solar wind disturbances. Event 1 is associated with a complicated shock-associated interplanetary coronal mass ejection (ICME) disturbance with large radial extent, probably formed by the merging of multiple shocks and transient flows, and which delivered a glancing blow to Earth. Conversely, Event 2 is accompanied by a relatively simple halo ICME with small radial extent that hit Earth more head-on. [4]

R. Jesus et. al. (2019) In this paper, we present the results of a morphological study of Equatorial Spread F (ESF) irregularities over Indian region based mainly on observations of (1) amplitude scintillations on GPS L-band signal and Rate of TEC Index (ROTI) obtained using a network of GPS receivers and (2) amplitude scintillations on a VHF signal using spaced receivers at Tirunelveli, an equatorial station. Occurrence of both amplitude scintillations on the GPS L1 signal and occurrence of significant ROTI recorded at several stations has been investigated. The latitudinal extent of L-band scintillations shows that their strength is weak over the dip equator but stronger over Equatorial Ionization Anomaly (EIA) region, preferentially during vernal equinox. We find an equinoctial asymmetry in both the occurrence of scintillations and ROTI wherein their occurrence is greater in the vernal equinox than in the autumn equinox. Attempts have been made to understand the asymmetry in latitudinal extent using maximum cross-correlation ($\mathbf{C_I}$) of intensity fluctuations obtained from the VHF spaced receivers observations. The observations suggest that occurrence of $\mathbf{C_I}$ less than 0.5 is

more in the vernal equinox than in the autumn equinox suggesting that the maximum height of the Equatorial Plasma Bubbles (EPBs) during vernal equinox may be higher than that during autumn equinox. [5]

3. PROPOSED METHODOLOGY

We analyze data from the NASA Wind spacecraft at times when it was in the upstream solar wind, accessed through the NASA/GSFC OMNI data set. Fifteen-second IMF data from the MFI instrument and 92 s plasma velocity data from SWE were combined to give a 1 min resolution time series prior to our access. The data are in the geocentric solar magnetospheric (GSM) coordinate system. We took 1 year of data around each of the minima and maxima of solar cycles 23 and 24, spanning periods 1 December 1995 to 30 November 1996 (cycle 23 minimum), 1 October 1999 to 30 September 2000 (cycle 23 maximum), 1 August 2007 to 31 July 2008 (cycle 24 minimum), and 1 November 2013 to 31 October 2014 (cycle 24 maximum). These dates were chosen based on the sunspot number, as in Hush et al. (2015).

Each year-long sample contains roughly 500,000 data points. Around 10% of the data is missing from each time series, with data gaps roughly evenly spread through the four samples, leaving around 450,000 points per year. The data are split into the fast and slow streams with a boundary at 450 kms^{-1}, chosen as the midpoint between the typical fast and slow wind speeds of ∼300 kms^{-1} and ∼600 kms^{-1}, respectively, to reduce as far as possible the contamination of slow wind data points into the fast wind data set and vice versa. This leaves around 150,000 data points in each fast wind sample and 300,000 in each slow wind sample. While the sample size in fast wind is significantly smaller than slow wind, both are sufficiently large to allow robust statistics for the DQQ method.

4. RESULTS AND DISCUSSION

DQQ Plots for Plasma Parameters

Data Set Combining Both Fast and Slow Wind: Resolving the More Extreme Values

We now apply the DQQ method to study the evolution of the distribution of (a) solar wind speed *v*, (b) IMF magnitude *B*, and (c) components of the magnetic field. In the discussion of the turbulent core of the distribution that follows, we will for conciseness plot the IMF *x* component B_x only, as in the core the *y* and *z* component behavior was found to be similar. The DQQ plots in show how the distribution of the full range of each of these parameters changes between the minima of cycles 23 and 24 (left column), the consecutive maxima (middle column), and between the maximum and minimum of each cycle (right column), for cycle 23 in red and cycle 24 in blue. Here we use all data available in each year-long sample, comprising

both fast and slow solar wind states. In most cases, more than 90% of the data fall into a single component, the "core" of the distribution. The remaining 10% of data form a distinct "tail" component, which itself splits into two parts in some cases.

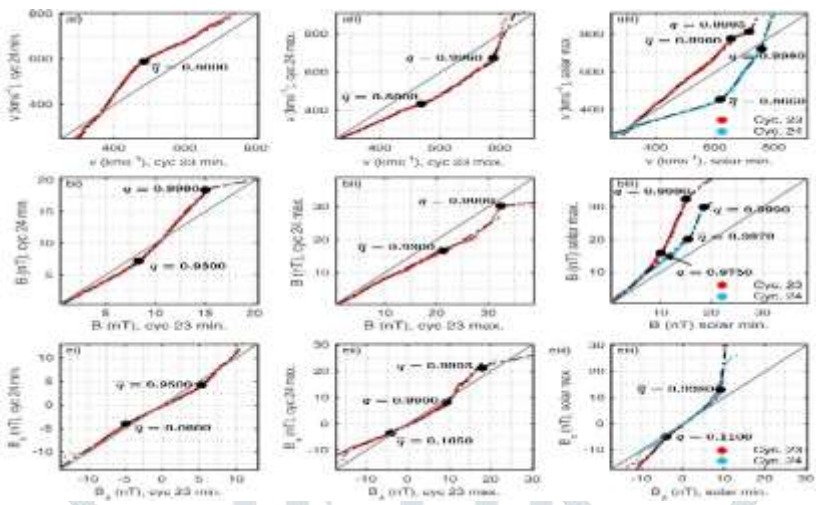

Focussing on Figures bi–biii, we see these differences between the cycles are reflected in the distribution of the magnetic field magnitude; Figure bii shows that the variance of all three components was larger at the maximum of cycle 23 than that of cycle 24, while in Figure 4biii we see a more marked change between the maximum and minimum of cycle 23 than 24, particularly in the extremal component. However, examining Figures ci–ciii we see changes in distribution are less clear for the *x* component of the field; notably in Figure ciii we see for both cycles 23 and 24 the core of the distribution of B_x, located between the $\bar{q}$ quantiles, did not change significantly between solar maximum and minimum.

Finally, inspecting the DQQ plots for solar wind speed in Figures ai–aiii, we notice a natural split in the distribution at $\bar{q}$ between 450 and 600 kms^{-1}. This is approximately the boundary between fast and slow solar wind, indicating that in distribution fast and slow wind transform differently over the solar cycles.

Separation of Fast and Slow Solar Wind

The DQQ plots for (a) *v*, (b) *B* and (c) B_x are shown in Figure for fast (left column) and slow (right column) wind separately. In each case we compare the $q = 0.0001$ to $q = 0.9999$ quantiles of the distribution of each parameter at solar maximum to those at solar minimum, for cycles 23 (red) and 24 (blue). The highlighted points now show the 0.9 and 0.99 quantiles in all cases, i.e., the values that exceed 90% and 99% of each sample. To split the data into the fast and slow states, we choose a constant threshold of 450 kms^{-1} and define fast wind as any single data point whose speed measurement exceeds this, giving 150,000 (300,000) points in each year-long fast (slow) wind sample. Of these, roughly 15,000 (30,000) exceed the 0.9 quantile, and 1,500 (3,000) exceed the 0.99 quantile.

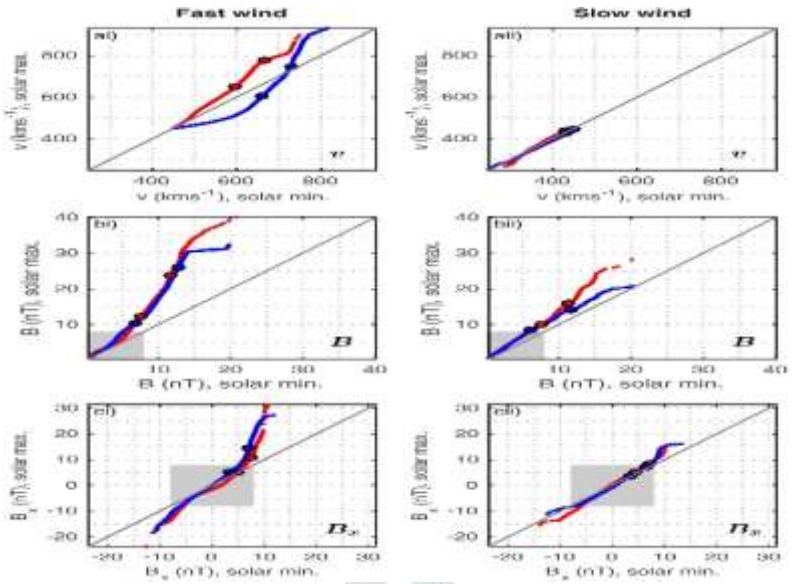

Solar Cycle Variation of the Distribution Core

To determine this range, we first split each year-long sample into 12 month-long samples, maintaining separate data sets for fast and slow solar wind. We then discard any month-long samples with fewer than 5,000 observations; these will have insufficient data to support an accurate estimate of the empirical distribution. A test lognormal distribution is constructed for each of the remaining monthly samples, with parameters estimated by taking the natural logarithm of the data and determining its mean and variance. The 12 month-long QQ traces from each year are superimposed on the same axes; row (a) shows the 12 months surrounding the minimum of cycle 23, row (b) shows the cycle 23 maximum, row (c) is the cycle 24 minimum and row (d) shows the cycle 24 maximum. As above, the left and right columns results for fast and slow wind, respectively.

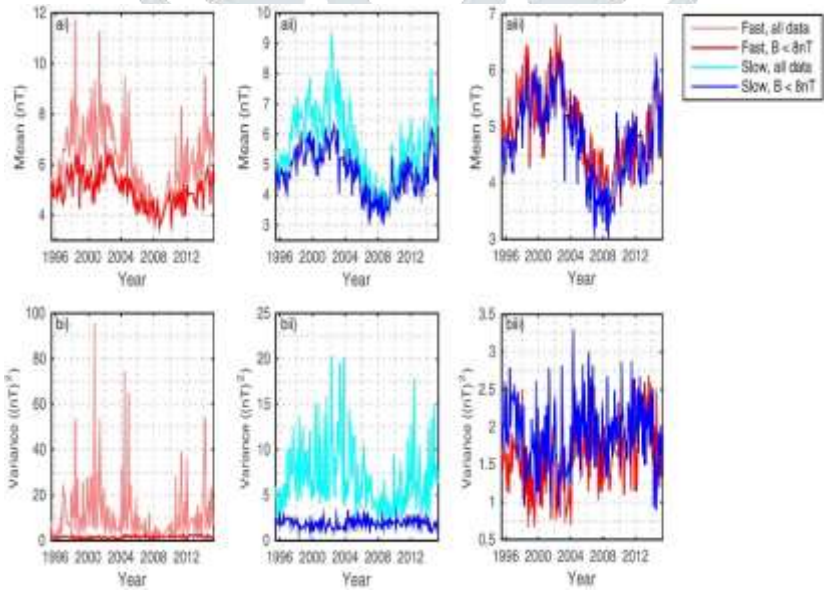

The time evolution of the mean (row a) and variance (row b) of month-long samples of IMF magnitude. Red lines denote properties of the fast wind data, while blue lines show slow wind properties. Light tones denote the moments of the full data set, whereas for darker shades only values in the core region (i.e., $B < 8$ nT) are considered.

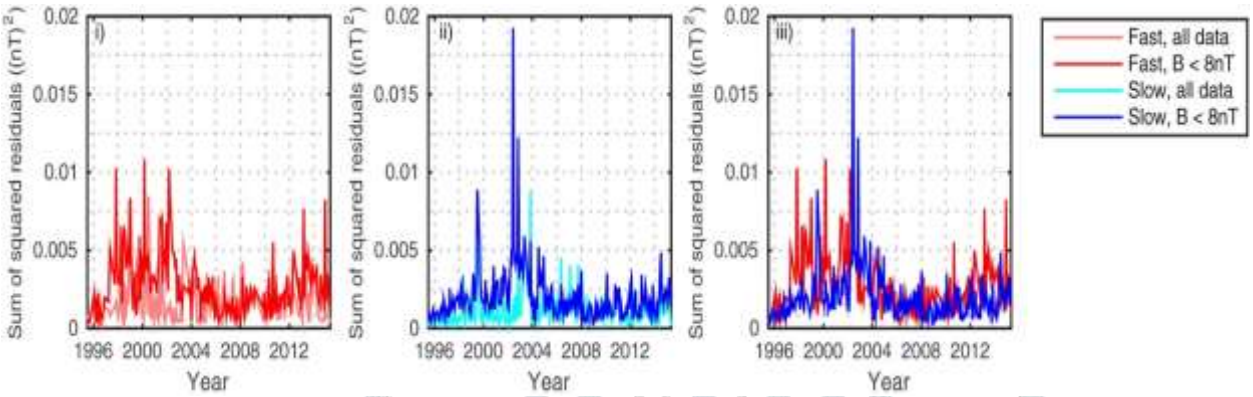

The normalized sum of squared residuals between the empirical PDF of month-long samples of the data and samples generated from a lognormal distribution with the same moments. Normalization is to the number of bins used to construct the empirical PDF.

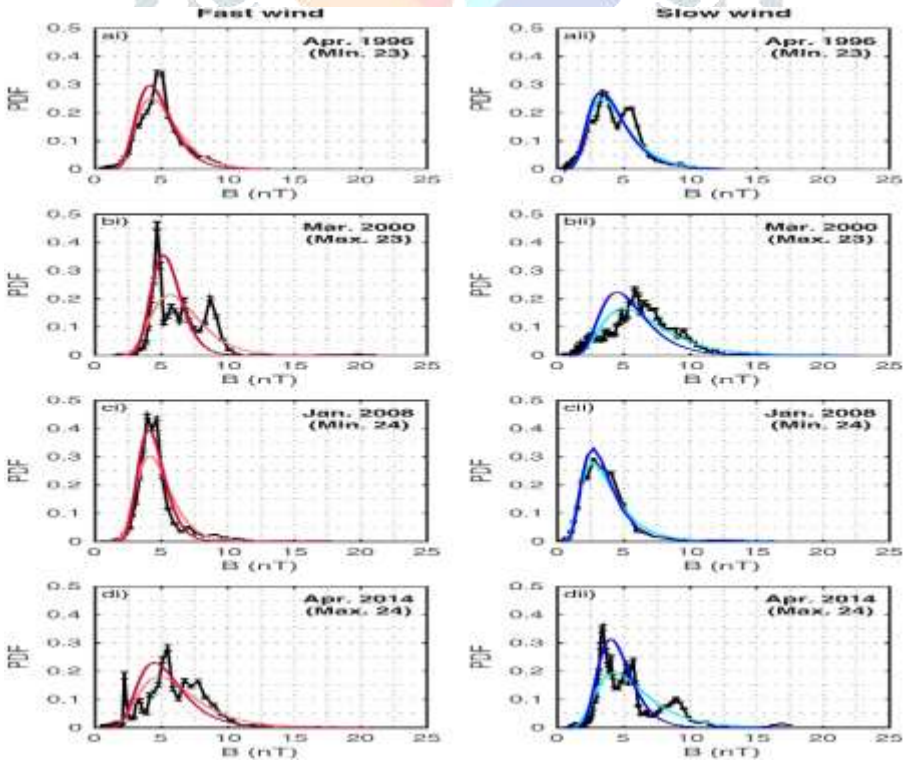

The empirical PDF of IMF field magnitude in (column i) fast and (column ii) slow wind, calculated from monthly data samples gathered in (a) April 1996, (b) March 2000, (c) January 2008, and (d) April 2014. The

PDF is given by the normalized histogram with logarithmically spaced bins; thus, its error is the square root of the number of samples in each bin.

5. Conclusion

The majority of the data falls into the core component; in this region the mean tracks the solar cycle while the variance fluctuates around a constant value, with the same variation seen in both solar cycles and both solar wind states. The largest $\backsim 10$% of observations form a distinct tail component, which varies in a distinguishable way between the distinct activity levels of the minimum and maximum of each solar cycle and also behaves differently in fast and slow solar wind. We find that the tail region becomes statistically dominant over the core for values above B = 8 nT ($|B_x|$=8 nT).

The core region of the IMF distribution is not sensitive to the distinct activity levels of the maximum and minimum of each cycle. This is consistent with an underlying in situ process modifying the evolution of small fluctuations in this region. when we test the lognormality of the core region over the solar cycle, we find that while the lognormal is a more robust description of the data in slow wind than fast across the solar cycle, in both solar wind states the lognormal most closely describes the data at solar minimum. At solar maximum, particularly in fast wind, the distribution exhibits multiple sharp peaks, and only in an interpolated sense follows a lognormal.

The extreme tail of the distribution is not captured by the lognormal model at any solar cycle phase, and excluding it from the data set used to create the lognormal model results in an improved correspondence to the core region at solar minimum. Unlike the turbulent core, the extremal component is sensitive to the differences in solar wind conditions in fast and slow solar wind seen at each distinct solar maximum and minimum.

6. References

[1] Dibyendu Nandy, Progress in Solar Cycle Predictions: Sunspot Cycles 24–25 in Perspective, Solar Physics, 10.1007/s11207-021-01797-2, **296**, 3, (2021).

[2] S.T. Lepri et. al. (2013), Solar wind heavy ions over solar cycle 23: ACE/SWICS measurements, The astrophysical journal, Volume 768, Number 1.

[3] E. Robbrecht *et al* 2009, Automated Lasco CME catalog for solar cycle 23: Are CMEs scale Invariant?, The astrophysical journal, Volume 691, Number 2.

[4] L.-L. Zhao et. al. 2016, Transient galactic cosmic-ray modulation during solar cycle 24 : A comparative study of two prominent forbush decrease events.

[5] R. Jesus, I. S. Batista, H. Takahashi, E. R. Paula, D. Barros, C. A. O. B. Figueiredo, A. J. Abreu, O. F. Jonah, P. R. Fagundes, K. Venkatesh, Morphological Features of Ionospheric

[6] Scintillations During High Solar Activity Using GPS Observations Over the South American Sector, Journal of Geophysical Research: Space Physics, 10.1029/2019JA027441, **125**, 3, (2020).

[7] Zhao, L. L., & Zhang, H. (2016). Transient galactic cosmic-ray modulation during solar cycle 24: A comparative study of two prominent Forbush decrease events. The Astrophysical Journal, 827(1), 13.

[8] Zhao, L., Zurbuchen, T. H., & Fisk, L. A. (2009). Global distribution of the solar wind during solar cycle 23: ACE observations. *Geophysical Research Letters*, *36*(14).